

Enhanced Density Fluctuations Near a Disordered Chiral Topological Transition

Hai-Tao Ding,^{1,2,*} Sen Mu,³ Leong-Chuan Kwek,^{1,2,4,5} Gabriel Lemarié,^{2,1,6,7,†} and Jiangbin Gong^{1,2,6,‡}

¹Centre for Quantum Technologies, National University of Singapore, 3 Science Drive 2, Singapore 117543

²MajuLab, CNRS-UNS-NUS-NTU International Joint Research Unit, Singapore UMI 3654, Singapore

³Max Planck Institute for the Physics of Complex Systems, Nöthnitzer Straße 38, 01187 Dresden, Germany

⁴National Institute of Education, Nanyang Technological University, Singapore 637616, Singapore

⁵Quantum Science and Engineering Centre (QSec), Nanyang Technological University, Singapore

⁶Department of Physics, National University of Singapore, 2 Science Drive 3, Singapore 117551, Singapore

⁷INPHYNI, Université Côte d'Azur, CNRS, Nice, France

The universal statistics of density fluctuations of localized quantum states may offer unprecedented opportunities to probe and understand quantum transport in connection with dimensionality, coherence, symmetry and disorder. To date, the possible role of topological phase transitions in the fluctuation statistics is not studied yet. Using a Su-Schrieffer-Heeger chain subject to off-diagonal disorder (so that chiral symmetry is preserved), this work investigates how a disorder driven topological phase transition impacts on the spatial fluctuations of the logarithmic wave-packet density $\ln P(r)$ at distance r from the initial excitation. Away from the transition, in both topological and trivial localized phases, the standard deviation follows the conventional one-dimensional scaling $\sigma[\ln P(r)] \sim r^\theta$ with $\theta \simeq 1/2$. Near the transition, however, the fluctuation growth is enhanced: the fitted exponent θ increases above $1/2$ in a nonmonotonic manner before returning close to $1/2$ at criticality. We interpret this behavior from the energy-resolved density of states and localization length. Near the transition, several energy sectors carry appreciable spectral weight and exhibit competitive decay rates, preventing a single localization scale from dominating the accessible wave-packet tail and thereby enhancing the fluctuations of $\ln P(r)$. Our results establish wave-packet fluctuation statistics as a dynamical diagnostic of disordered chiral topological transitions and motivate broader studies of fluctuation phenomena in disordered topological quantum systems.

I. INTRODUCTION

The interplay of topology and disorder has attracted intense interest in modern condensed matter physics. Disorder can destroy, reshape, or even generate topological phases. A prominent example is the topological Anderson insulator [1], which has recently been realized experimentally in disordered topological systems [2–14]. These phases are usually characterized through topological invariants, boundary modes, and transport responses [1, 15–19]. However, much less is known about how a disorder-driven topological phase transition may be manifested and probed in the statistical aspects of localized quantum states. This question is particularly natural because Anderson localization is intrinsically statistical: even when the mean profile is exponentially localized, the density or its logarithm can fluctuate strongly from one disorder realization to another.

In disordered quantum systems, universal fluctuation phenomena are often discussed within random-matrix and transfer-matrix frameworks [20–22]. Random-matrix theory provides a statistical description of spectral correlations, scattering matrices, and mesoscopic transport fluctuations after microscopic details are coarse grained [20, 23]. In quasi-one-dimensional systems, the Dorokhov-Mello-Pereyra-Kumar equation describes the

stochastic evolution of transmission eigenvalues, or the associated Lyapunov exponents, with increasing sample length [21, 24–29]. In the localized regime, products of transfer matrices naturally lead to additive fluctuations in logarithmic quantities, including wave-function amplitudes and densities [21, 22]. As a result, the logarithmic density $\ln P(r)$ of localized states exhibits universal scaling behavior. In one or quasi-one dimension, $\ln P(r)$ at large distance r from the localization center scales as $\sigma[\ln P(r)] \sim r^{1/2}$ [30–33]. In two dimensions, logarithmic density or conductance fluctuations are instead connected to the Kardar-Parisi-Zhang universality class [34] with $\sigma[\ln P(r)] \sim r^{1/3}$ [35–40]. These results show that fluctuation statistics provide a refined characterization of localized states, beyond the mean exponential decay. Since topology and symmetry impose additional structure on localization, it is natural to ask whether such fluctuation statistics are modified across a disordered topological phase transition. This question is the focus of the present work.

A minimal setting for this question is provided by the one-dimensional Su-Schrieffer-Heeger (SSH) chain with off-diagonal disorder [41]. In Anderson localization with onsite disorder, all eigenstates are exponentially localized in one dimension [32, 42–46]. By contrast, off-diagonal (hopping) disorder preserving chiral symmetry gives the zero-energy sector a special role. While eigenstates at non-zero energy remain exponentially localized, the zero-energy states can display anomalous behavior, including divergent localization length and sub-exponential typical profiles at criticality [47–59]. The coexistence of ordinary exponentially localized finite-energy states and non-

* htting.9@nus.edu.sg

† gabriel.lemarie@cnrs.fr

‡ phygj@nus.edu.sg

trivial (near)-zero-energy states suggests that the spatial fluctuations of a time-evolved wave packet may provide a sensitive probe of the chiral topological transition.

In this work, we study the long-time density profile of a wave packet initially localized in a single unit cell of a disordered SSH chain. We focus on the disorder-induced fluctuations of $\ln P(r)$, an experimentally accessible quantity obtained from the spatial probability profile of the evolved wave packet, as a function of the distance r from the initial excitation. In both the topological and trivial localized phases away from the transition, we find the conventional one-dimensional scaling $\sigma[\ln P(r)] \sim r^\theta$ with $\theta \simeq 1/2$. Near the transition, however, the fluctuation growth is enhanced: the numerically fitted exponent rises above $1/2$ in a nonmonotonic manner, before returning close to $1/2$ at the critical point. This behavior shows that the strongest fluctuation enhancement does not occur exactly at criticality, but rather in the near-critical regime. Exactly how the above-mentioned growth exponent of the fluctuation statistics behaves near a topological phase transition will be investigated computationally in this work.

We interpret this nonmonotonic behavior in terms of energy-resolved localization. The two relevant ingredients are the disorder averaged density of states $\langle \rho(E) \rangle$, which determines the density of available states in different energy sectors, and the localization length $\xi(E)$, which determines their decay rates. Away from the transition, the relevant energy sectors have comparable decay rates, so the wave-packet tail is effectively governed by a narrow range of localization scales, leading to the conventional scaling $\sigma[\ln P(r)] \sim r^{1/2}$. Near the transition, the disorder averaged density of states and localization-length spectrum indicate that several energy sectors contribute with appreciable spectral weight and distinct decay rates. As a result, no single localization scale dominates the wave-packet tail over the accessible distances, and this competition enhances the fluctuation growth of $\ln P(r)$. At the critical point, by contrast, the sharp zero-energy sector provides a cleaner dominant contribution, restoring a fluctuation exponent close to the conventional value despite the sub-exponential typical spatial profile. Our results establish wave-packet fluctuation statistics as a dynamical diagnostic of disordered chiral topological transitions and motivate broader studies of fluctuation phenomena in topological Anderson systems.

The paper is organized as follows. In Sec. II, we define the disordered SSH model, characterize its real-space winding number, and locate the chiral topological transition using both numerical and transfer-matrix diagnostics. In Sec. III, we present the long-time wave-packet profiles and the fluctuation scaling of $\ln P(r)$ across the topological, topological-Anderson, critical, and trivial regimes. In Sec. IV, we develop the energy-resolved interpretation of the enhanced fluctuation exponent in terms of the disorder averaged density of states and localization-length spectrum. We conclude in Sec. V with a summary and outlook.

II. DISORDERED SSH MODEL AND ITS PHASE DIAGRAM

We consider a disordered SSH model with random intracell hopping [41]

$$H = \sum_{i=1}^N t_{1,i} a_i^\dagger b_i + \sum_{i=1}^{N-1} t_2 a_{i+1}^\dagger b_i + \text{H.c.}, \quad (1)$$

where H.c. denotes the Hermitian-conjugate term. a_i^\dagger (b_i^\dagger) and a_i (b_i) are the creation and annihilation operators for sublattice A (B) in the i -th unit cell, respectively. t_2 is the intercell hopping strength. $t_{1,i}$ is the intracell hopping strength with $t_{1,i} = t_1 + \delta W$, t_1 is the mean intracell hopping strength, and δW are independent random numbers chosen uniformly in the range $[-W, W]$. Such hopping disorder breaks the discrete translational invariance of the system, but preserves the chiral symmetry $\Gamma H \Gamma^{-1} = -H$, where the chiral symmetry operator is defined as $\Gamma = I_N \otimes \sigma_z$, with I_N the $N \times N$ identity matrix and σ_z the 2×2 Pauli- z matrix.

A. Real-space winding number

The topology of the disordered chain can be characterized by the real space winding number [49, 60]

$$v = \frac{1}{L'} \text{Tr}'(\Gamma Q[Q, X]). \quad (2)$$

Here, $Q = \sum_{j=1}^N (|j\rangle\langle j| - |\tilde{j}\rangle\langle \tilde{j}|)$, with $|j\rangle$ and $|\tilde{j}\rangle$ are the conductance band and the valence band respectively, X is the coordinate operator, and Tr' denotes the trace over the central segment of the lattice of length $L' = N$, with N is the number of the unit cell. Unless otherwise specified, we employ the periodic boundary condition (PBC) throughout this paper. The topological phase diagram of the disordered SSH model depicted in Eq. (1) as the function of W and t_1 is shown in Fig. 1(a).

The lower-left region is the conventional topological insulator (TI) phase with winding number $v = 1$. In addition, the phase diagram contains a disorder-induced topological Anderson insulator (TAI) phase [1–4, 6, 8–10, 15–19], which also has $v = 1$ but emerges from a regime that is trivial in the clean limit. The rest region of Fig. 1(a) is the normal insulator (NI) phase with $v = 0$.

B. Zero-energy transfer-matrix recursion

The above phase transition can also be analytically found from the zero-energy transfer-matrix recursion [32, 49], which yields

$$\gamma(E = 0) \equiv \lim_{N \rightarrow \infty} \frac{1}{N} \sum_{i=1}^N \ln \left| \frac{t_{2,i}}{t_{1,i}} \right|, \quad (3)$$

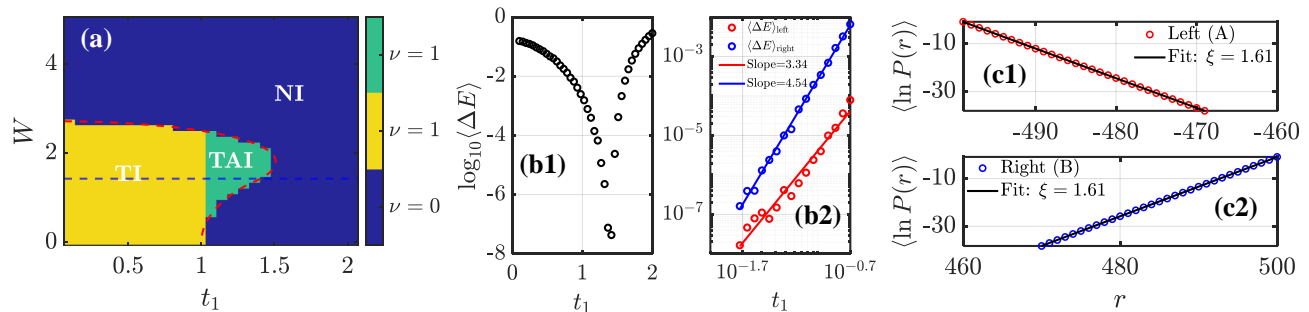


FIG. 1. (a) The phase diagram in the (t_1, W) plane. Both TI and TAI regions are characterized by winding number $\nu = 1$, while the NI region has $\nu = 0$. The TAI phase is distinguished from the TI phase in that it is disorder-induced from a regime that is trivial in the clean limit. Analytically derived phase boundary from zero-energy transfer-matrix recursion is shown with the red dashed line, see [49, 61] and Appendix A for more details. (b1-b2) Disorder-averaged energy gap $\log_{10}\langle\Delta E\rangle$ as a function of t_1 , with $W = 1.43$. (b1) $t_1 \in (0.1, 2)$, the gap closing at the transition point $t_1^c = 1.40$; (b2) Scaling of the disorder-averaged energy gap $\langle\Delta E\rangle$ versus $|t_1 - t_1^c|$ on a double-logarithmic scale. The left and right branches are shown by red and blue circles, respectively. Solid lines are linear fits in log scale, corresponding to power-law exponents 3.34 and 4.54. (c1-c2) Disorder-averaged profiles $\langle \ln P(r) \rangle$ of the left and right topological edge states, with $t_1 = 0.29$ and $W = 1.43$. Here r is the unit-cell index. To display the two edge states in a unified way, the profile of the left-edge state is plotted on the negative- r side, while that of the right-edge state is plotted on the positive- r side. (c1) Profile of the left edge state, localized near the left boundary and residing exclusively on the sublattice A. (c2) Profile of the right edge state, localized near the right boundary and residing exclusively on the sublattice B. Solid lines are exponential fits, yielding the same localization length $\xi = 1.61$ for both edge states, which is consistent with the analytical result obtained from the zero-energy transfer-matrix recursion [49, 61], see Appendix A for more detail. Here the intercell hopping strength $t_2 = 1$, the number of unit cell is $N = 10^3$. Results under periodic boundary conditions are shown in (a) and (b), while (c) shows the corresponding result under open boundary conditions.

with $t_{1,i} = t_1 + \delta W$ and $t_{2,i} = t_2$. Here $\gamma(E = 0)$ is the signed Lyapunov exponent at zero energy [32, 49]. For the topological phases, $\gamma(E = 0) > 0$, and the zero-energy edge states are exponentially localized at the two edges with localization length $\xi(E = 0) = 1/\gamma(E = 0)$; For the trivial insulator phase, $\gamma(E = 0) < 0$, so the zero-energy solution is non-normalizable and therefore does not represent a physical edge state. The topological phase transition occurs at $\gamma(E = 0) = 0$, and the localization length diverges [49, 61]. We analytically derive the phase boundary shown in Fig. 1(a) with the red dashed line [49]; it is consistent with the topological phase boundary numerically determined from the real space winding number, see Appendix A for more details.

C. Disorder-averaged energy gap

We then calculate the disorder averaged energy gap $\langle\Delta E\rangle$, here $\langle \dots \rangle$ represents the average over disorder realizations. The results of $\log_{10}\langle\Delta E\rangle$ are shown in Fig. 1(b1). The topological Anderson insulator phase is gapped, although the gap remains small. The topological phase transition occurs at the gapless point where the gap closes and reopens, with $t_1^c = 1.40$ when the disorder strength $W = 1.43$ (The blue dashed line in Fig. 1(a) is for $W = 1.43$). In Fig. 1 (b2), we present the gap on a log-log scale as a function of the distance to the critical point (CP), $|t_1 - t_1^c|$, taking from both sides. The red circles (blue circles) correspond to approaching t_1^c from $t_1 < t_1^c$ ($t_1 > t_1^c$): they exhibit power-law scaling

$$\langle\Delta E\rangle \propto |t_1 - t_1^c|^\nu, \text{ with } \nu = 3.34 \text{ (4.54) when } t_1 \rightarrow t_1^c.$$

D. Disorder-averaged logarithmic density of zero-energy edge states

In Fig. 1(c1-c2), we also examine the disorder averaged logarithm of the density distribution $\langle \ln P(r) \rangle$ of two zero-energy edge states with open boundary condition (OBC). $P(r)$ is the total probability density within the r -th unit cell, defined as the sum over the density distribution of two sublattices A and B: $P(r) = |\psi_A(r)|^2 + |\psi_B(r)|^2$. The left and right edge states are localized at the corresponding boundaries and reside exclusively on the A and B sublattices, respectively. Both zero-energy states under OBC decay with the same localization length, $\xi=1.61$, consistent with the analytical result obtained from the zero-energy transfer-matrix recursion in Eq. (3) [49, 61], see Appendix A for more details.

III. WAVE-PACKET LOCALIZATION AND FLUCTUATION SCALING ACROSS THE CHIRAL TRANSITION

For the one-dimensional Anderson model with uncorrelated onsite disorder, all eigenstates are exponentially localized for arbitrarily weak disorder [32, 42–46]. A wave packet launched from a localized initial state therefore remains spatially confined at long times [22, 32, 62, 63]. In

the chiral symmetric SSH chain, finite-energy states are also exponentially localized, but the zero-energy sector becomes anomalous at the topological transition: its localization length diverges and its typical profile becomes sub-exponential [48–50], see Appendix B for more details. This motivates a direct study of the long-time wave-packet spatial profile and its fluctuations across disorder realizations.

A. Localization of the wave packets

We consider an initial state localized at the center of the chain, specifically in the $N/2$ -th unit cell, with N the number of unit cells. The state vector is defined as $\psi_{\text{ini}} = (0, \dots, 1/\sqrt{2}, 1/\sqrt{2}, \dots, 0)^T$. Subsequently, the time evolution is governed by the Hamiltonian in Eq. (1), under the periodic boundary condition, thereby avoiding any possible artificial effect from the boundary. To investigate the long-time localization behavior of the wave packet, we analyze the disorder-averaged logarithmic density $\langle \ln |P(r)| \rangle$, where $P(r) = |\psi(r)|^2$ and r denotes the distance from the initial excitation. We numerically simulate the evolution of the wave packet for four different intracell hopping strength t_1 in Fig. 2 (a-d): $t_1 = 0.29$ (deep in TI), $t_1 = 1.12$ (TAI), $t_1 = 1.40$ (CP), $t_1 = 1.90$ (deep in NI). As shown in Fig. 2 (a,b,d), the wave packets exhibit exponential localization $\langle \ln P(r) \rangle \approx -2r/\xi + \text{const}$, with ξ the localization length. Note the absence of $E = 0$ eigenstates in these three regimes, so that all eigenstates are expected to be exponentially localized [48–50]. However, for the case of $t_1 = 1.40$ shown in Fig. 2 (c), the wave packet does not approach a stationary profile even in the long-time limit ($T_3 = 10^5$) we considered, reflecting some anomalous critical nature of the states, likely connected with the $E = 0$ eigenstates at the transition point, whose typical spatial profile decays subexponentially [48–50].

B. Fluctuation scaling of the logarithmic wave-packet density as a function of the distance

We now consider the fluctuations statistics of the logarithmic wave-packet density. For standard Anderson localization, the fluctuation statistics follows the scaling $\sigma[\ln P(r)] \sim r^{1/2}$ in 1D [30–33], whereas in 2D it follows the Kardar-Parisi-Zhang scaling $\sigma[\ln P(r)] \sim r^{1/3}$ [34–38, 40, 64–66]. Motivated by these results, we examine whether and how the fluctuation scaling is modified in the present chiral-symmetric SSH model across the topological transition. To this end, note that $\langle \ln P(r) \rangle$ describes the typical decay profile, the standard deviation of $\ln P(r)$,

$$\sigma[\ln P(r)] = \sqrt{\langle (\ln P(r))^2 \rangle - \langle \ln P(r) \rangle^2}. \quad (4)$$

quantifies how the distribution broadens across disorder realizations as the distance r increases, and we fit our

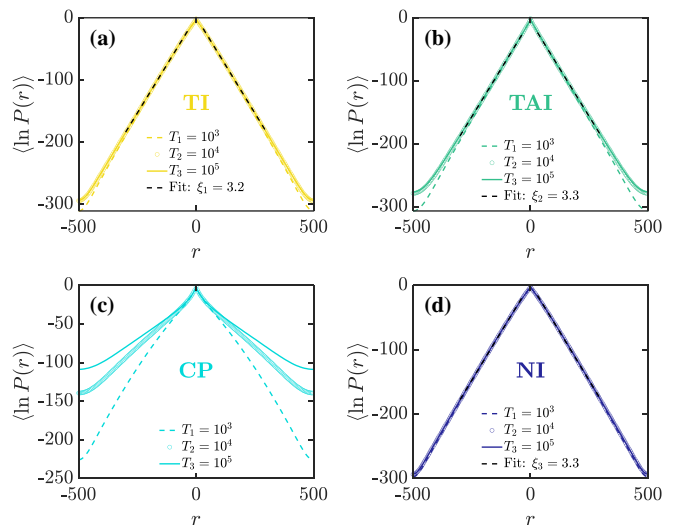


FIG. 2. Disorder-averaged logarithm of the wave density $\langle \ln P(r) \rangle$ at three evolution times, $T_1 = 10^3$, $T_2 = 10^4$, $T_3 = 10^5$, for four representative values of t_1 . (a) $t_1 = 0.29$ (TI), the profiles at different times nearly collapse and are well fitted by an exponential decay, with the localization length $\xi = 3.2$. (b) $t_1 = 1.12$ (TAI), the profiles also approach a common exponential form at long times, with the localization length $\xi = 3.3$. (c) The disorder-averaged logarithm of the wave density for $t_1 = t_1^c = 1.40$ at the critical point (CP), the profile exhibits pronounced time dependence and deviates markedly from a simple exponential form, due to the subexponential decay of the typical profile associated with the $E = 0$ eigenstates. (d) $t_1 = 1.90$ (NI), the long-time profile remains exponentially localized, similar to the other insulating phases, with the localization length $\xi = 3.3$. Other parameters are $t_2 = 1$, $N = 10^3$, $N_d = 10^4$, $W = 1.43$.

numerical results to

$$\sigma[\ln P(r)] \sim r^\theta. \quad (5)$$

In Fig. 3 (a-d), we present our numerical results for different values of t_1 focusing on the fitted growth exponent θ . In the localized TI and NI regimes away from the transition, we find $\theta \simeq 1/2$ once r exceeds the fitted localization length. Thus, despite the chiral symmetry and the distinct topological character of the phases, the long-distance fluctuation scaling agrees with the standard one-dimensional Anderson result. Interestingly, at the critical point $t_1 = t_1^c$, although the wave packet is not exponentially localized, the fitted fluctuation exponent remains close to $1/2$.

Remarkably, the strongest deviation appears near, but not exactly at, the transition. For $t_1 = 1.12$ in the TAI regime, the growth exponent is as large as $\theta = 0.65$. To further characterize the fluctuation scaling behavior across the topological phase transition, we extract the exponent θ from the fitted scaling relation $\sigma[\ln P(r)] \sim r^\theta$ for different t_1 . As summarized in Fig. 3 (e), as t_1 approaches the critical point ($t_1 = t_1^c$), θ increases above $1/2$ as the transition is approached, but then drops back

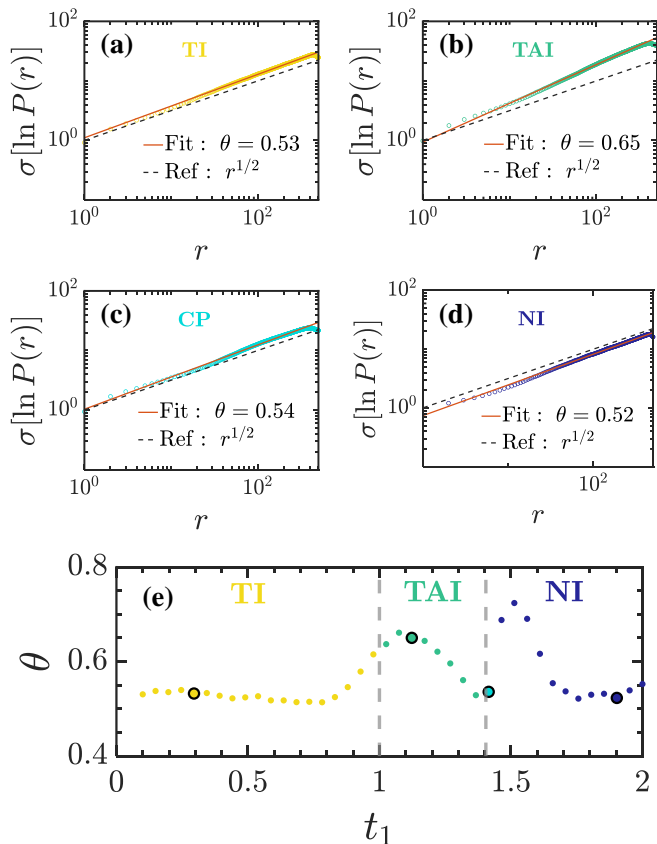


FIG. 3. The fluctuation of the logarithm of the wave density $\ln P(r)$ with distance r . The blue circles represent the numerical data, the solid red line shows a power-law fit, the black dashed line indicates the scaling $y = r^{1/2}$ for reference. (a) $t_1 = 0.29$ (TI), the growth exponent is 0.53. (b) $t_1 = 1.12$ (TAI), the growth exponent is 0.65. (c) $t_1 = 1.40$ (CP), the growth exponent is 0.54. (d) $t_1 = 1.90$ (NI), the growth exponent is 0.52. (e) Fitted growth exponent θ as function of the mean intracell hopping strength t_1 . The four black open circles in panel (e) mark the four representative values of t_1 used in panels (a)–(d). The two dashed vertical lines separate the TI, TAI, and NI regimes. Other parameters are $t_2 = 1$, $N = 10^3$, $N_d = 10^4$, $W = 1.43$.

to a value close to $1/2$ at $t_1 = t_1^c$. This nonmonotonic behavior is the central observation of this work. We have also checked larger systems with $N = 5000$, finding results consistent with those for $N = 1000$; further details are provided in Appendix C.

IV. ENHANCED FLUCTUATION SCALING FROM ENERGY-SECTOR SELECTION

For a one-dimensional localized eigenstate at energy E , the logarithmic density at distance r from the localization center can be written as

$$\ln P_E(r) \simeq -2r/\xi(E) + \delta h_E(r), \quad (6)$$

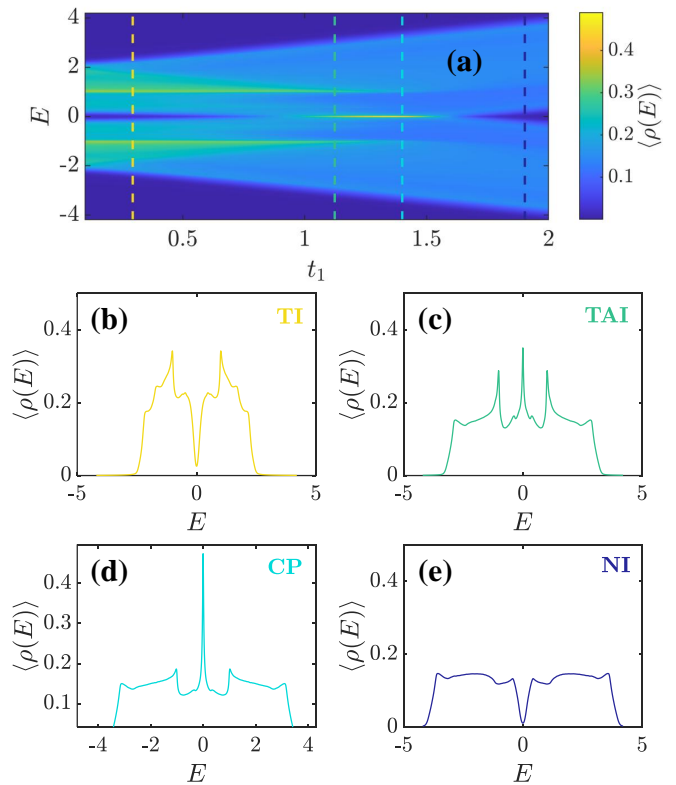


FIG. 4. Disorder-averaged density of states $\langle \rho(E) \rangle$ across the chiral topological transition. (a) $\langle \rho(E) \rangle$ as a function of the mean intracell hopping strength t_1 and energy E . The four vertical dashed lines mark four representative values of t_1 used in panels (b)–(e). (b)–(e) Energy dependence of $\langle \rho(E) \rangle$ for $t_1 = 0.29$ (TI), $t_1 = 1.12$ (TAI), $t_1 = 1.40$ (CP), and $t_1 = 1.90$ (NI), respectively. At $t_1 = 1.12$, the system is still gapped, and the central peak corresponds to near-zero-energy states rather than states exactly at $E = 0$. At the critical point $t_1 = 1.40$, the gap closes and the sharp peak occurs at $E = 0$. In the near-critical TAI regime, spectral weight appears both near zero energy and finite-energy sectors, indicating the coexistence of several relevant energy channels. At the critical point, the density of states is dominated by a sharp zero-energy contribution. Other parameters are $t_2 = 1$, $N = 10^3$, $N_d = 10^4$, and $W = 1.43$.

where $\xi(E)$ is the localization length, and $\delta h_E(r)$ denotes the accumulated random fluctuation of the logarithmic density [30, 32, 33]. For a fixed energy sector, this fluctuation obeys the conventional one-dimensional scaling $\sigma[\delta h_E(r)] \sim r^{1/2}$ [30–33]. For a time-evolved wave packet, the long-distance tail is determined by the energy sectors selected by their spectral weight and localization length $\xi(E)$. If several sectors with distinct localization lengths contribute simultaneously, the tail is no longer governed by a single decay channel, and the fluctuation of $\ln P(r)$ is enhanced.

This motivates an energy-resolved analysis of the competing sectors. We therefore compute the disorder-averaged density of states $\langle \rho(E) \rangle = \langle \frac{1}{2N} \sum_n \delta(E - E_n) \rangle$ and the energy-resolved localization length $\xi(E)$, shown

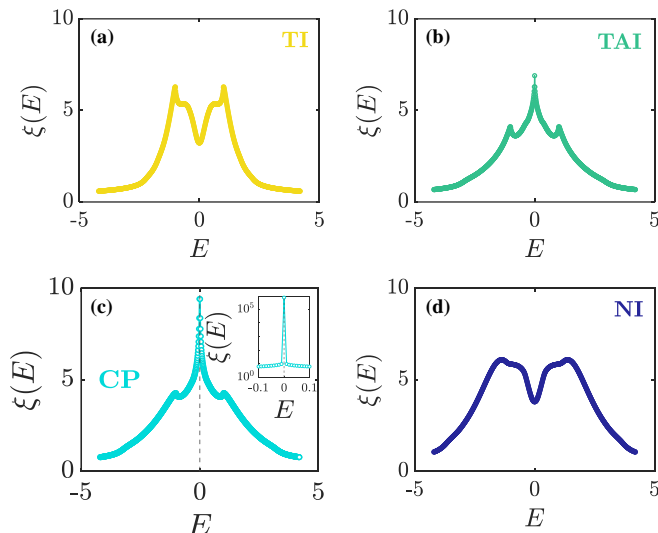


FIG. 5. The energy-resolved localization length $\xi(E)$ for four representative values of t_1 . (a) $t_1 = 0.29$ (TI). (b) $t_1 = 1.12$ (TAI). (c) $t_1 = 1.40$ (CP). (d) $t_1 = 1.90$ (NI). The localization length is obtained from the inverse magnitude of the disorder-averaged Lyapunov exponent. In the TI and NI regimes, $\xi(E)$ remains finite over the relevant energy range, indicating that the long-distance wave-packet tail is governed by a stable effective decay scale. In the near-critical TAI regime, several energy sectors have comparable but distinct localization lengths, so the tail is not selected by a single decay channel; this competition accounts for the enhanced fluctuation of $\ln P(r)$. At the critical point, $\xi(E)$ diverges at $E = 0$, reflecting the vanishing zero-energy Lyapunov exponent and showing that the zero-energy sector controls the long-distance dynamics. In panel (c), the main plot uses a linear scale to display the finite-energy structure, whereas the inset shows the same data near $E = 0$ on a logarithmic scale, highlighting the divergent zero-energy localization length. Other parameters are $t_2 = 1$, $N_d = 10^4$, and $W = 1.43$.

in Fig. 4 and Fig. 5, respectively. In the deep topological localized regime, represented by $t_1 = 0.29$, the disorder averaged density of states [Fig. 4(b)] is concentrated in finite-energy regions ($E \approx \pm 1$), while the localization-length spectrum [Fig. 5(a)] selects a well-defined finite-energy localization scale ($\xi(E = 1) = \xi(E = -1)$). Although many eigenstates contribute to the wave packet, its long-distance tail is effectively governed by a single dominant decay channel. The fluctuation of $\ln P(r)$ therefore follows the ordinary one-dimensional scaling $\sigma[\ln P(r)] \sim r^{1/2}$.

The situation is different in the near-critical topological Anderson regime, represented by $t_1 = 1.12$ [Fig. 4(c) and Fig. 5(b)]. In this regime, the system remains gapped, but spectral weight accumulates near zero energy while finite-energy sectors remain appreciable. The corresponding localization lengths also vary significantly among these energy windows. As a result, the wave-packet tail is not selected by a single localization scale. Instead, several energy sectors with distinct localization lengths contribute simultaneously, which enhances the

growth of $\sigma[\ln P(r)]$ and gives rise to an apparent exponent larger than $1/2$.

The critical point, $t_1 = t_1^c = 1.40$, should be distinguished from the near-critical competition regime discussed above. At criticality, both $\langle \rho(E) \rangle$ and $\xi(E)$ exhibit a sharply resolved zero-energy sector, as shown in Fig. 4(d) and Fig. 5(c). The gap closes and the localization length $\xi(E = 0)$ diverges, so the long-time wave-packet tail is dominated solely by the zero-energy sector. At this critical point, we observe $\sigma[\ln P(r)] \sim r^{1/2}$. This scaling may be inferred from the zero-energy-state analysis of one-dimensional random-hopping chains [49, 61, 67].

Deep in the trivial localized phase ($t_1 = 1.90$), the zero-energy singularity is absent, and all relevant localization lengths remain finite. The disorder averaged density of state [Fig. 4(e)] varies smoothly over relevant energy window, while $\xi(E)$ [Fig. 5(d)] shows only moderate energy dependence. As a result, the wave-packet tail is not affected by a sharp accumulation of zero-energy states or by a broad competition among different localization scales. The decay is therefore effectively governed by a relatively narrow range of localization lengths, and the usual one-dimensional localization fluctuation scaling $\sigma[\ln P(r)] \sim r^{1/2}$, is recovered.

The resulting picture is therefore not that the fluctuation exponent is controlled simply by the magnitude of the localization length or by the accumulation of near-zero energy states alone. Instead, it is determined by whether the density of states and the energy-resolved localization length favor a narrow range of effective decay channels, or whether several channels with comparable spectral weight and distinct decay rates compete. Away from the transition, the wave-packet tail is effectively controlled by a narrow range of localization scales. At the critical point, the sharp zero-energy sector provides the dominant long-distance contribution. The strongest enhancement appears in the near-critical gapped regime, where near-zero and finite-energy sectors coexist with appreciable spectral weight and distinct localization lengths. Their simultaneous contribution prevents the accessible tail from being governed by a narrow set of effective decay channels, thereby enhancing the fluctuation growth of $\ln P(r)$.

V. CONCLUSION AND DISCUSSION

We have studied the spatial fluctuation statistics of a long-time wave packet in a disordered SSH chain with chiral symmetry. The central observable is the logarithmic wave packet density $\ln P(r)$, whose standard deviation characterizes the sample-to-sample fluctuations of localized wave packet tails. In the topological and trivial localized phases away from the transition, the fluctuation scaling follows the conventional one-dimensional form $\sigma[\ln P(r)] \sim r^{1/2}$. This indicates that topology alone does not necessarily modify the scaling of loga-

rhythmic density fluctuations when the wave-packet tail is governed by a relatively narrow range of localization scales. However, the fluctuation growth is enhanced in the vicinity of the chiral topological transition, but returns close to $1/2$ at the critical point.

The enhancement originates from the energy-resolved structure of the localized states. In the near-critical regime, localized components with different decay lengths contribute simultaneously to the wave-packet tail, giving rise to a multi-scale decay structure that amplifies the fluctuations of $\ln P(r)$. At criticality, by contrast, the zero-energy sector dominates the long-distance dynamics. As a result, the fitted fluctuation exponent returns close to $1/2$, even though the wave-packet profile itself remains anomalous.

Several directions naturally follow from these results. One direction is to extend the analysis to disordered systems in different symmetry classes, with the aim of identifying which aspects of the enhanced fluctuation scaling are specific to chiral symmetry and which reflect more general consequences of symmetry-controlled criticality. Another important direction is to study higher-dimensional chiral and topological Anderson systems. We speculate that, in two-dimensional chiral-symmetric disordered systems, chiral symmetry may play an important role in fluctuation statistics, potentially leading to deviations from the Kardar-Parisi-Zhang scaling.

ACKNOWLEDGMENTS

The authors thank Christian Miniatura, Maxime Richard, Hui Khoon Ng, and Zhixing Zou for helpful discussions. We acknowledge the use of computational resources at the Singapore National Super Computing Centre (NSCC) ASPIRE-2A cluster, at Calcul en Midi-Pyrénées (CALMIP) for our simulations. This work is supported by the Singapore Ministry of Education Academic Research Funds Tier II (MOE-T2EP50223-0009 and MOE-T2EP50222-0005), by France 2030 under the French National Research Agency Award QUTISYM No. ANR-23-PETQ-0002 and by the ANR Research Grants ManyBodyNet No. ANR-24-CE30-5851. J.G. also acknowledges support by the National Research Foundation, Singapore, through the National Quantum Office, hosted in A*STAR, under its Centre for Quantum Technologies Funding Initiative (S24Q2d0009).

Appendix A: Analytical Derivation of $\gamma(0)$ from the $E = 0$ transfer matrix recursion

We provide a rigorous derivation of $\gamma(0)$ for the 1D off-diagonal disordered SSH model [49, 61]. We first introduce the general transfer matrix formalism and then demonstrate how the zero-energy condition simplifies the problem, allowing for an exact analytical solution. We

consider the one-dimensional SSH model with uncorrelated intercell hopping [2, 41], defined as:

$$H = \sum_n (t_{1,n}|n, A\rangle\langle n, B| + t_{2,n}|n, B\rangle\langle n+1, A| + \text{h.c.}), \quad (\text{A1})$$

where $|n, A\rangle$ and $|n, B\rangle$ denote the states on the two sublattices (A and B) in the n -th unit cell. $t_{1,n}$ represents the intra-cell hopping, and $t_{2,n}$ represents the inter-cell hopping. The Schrödinger equation $H|\psi\rangle = E|\psi\rangle$ for a state $|\psi\rangle = \sum_n (a_n|n, A\rangle + b_n|n, B\rangle)$ yields the following coupled equations for the amplitudes a_n and b_n :

$$Ea_n = t_{1,n}b_n + t_{2,n-1}b_{n-1}, \quad (\text{A2})$$

$$Eb_n = t_{1,n}a_n + t_{2,n}a_{n+1}. \quad (\text{A3})$$

At zero energy ($E = 0$), a significant simplification occurs due to the chiral (sublattice) symmetry of the bipartite lattice. Setting $E = 0$ in Eqs. (A2) and (A3), the equations for the two sublattices decouple completely:

$$0 = t_{1,n}b_n + t_{2,n-1}b_{n-1} \implies b_n = -\frac{t_{2,n-1}}{t_{1,n}}b_{n-1}, \quad (\text{A4})$$

$$0 = t_{1,n}a_n + t_{2,n}a_{n+1} \implies a_{n+1} = -\frac{t_{1,n}}{t_{2,n}}a_n. \quad (\text{A5})$$

This decoupling implies that the zero-energy eigenstates are confined to either the A-sublattice or the B-sublattice. By iterating these two relations from the first unit cell to the N -th unit cell, the amplitudes a_N and b_N are expressed as a product of hopping ratios:

$$a_N = \prod_{i=1}^{N-1} \left(-\frac{t_{1,i}}{t_{2,i}} \right) a_1, \quad (\text{A6})$$

$$b_N = \prod_{i=2}^N \left(-\frac{t_{2,i-1}}{t_{1,i}} \right) b_1.$$

In the zero-energy transfer-matrix recursion, the amplitude ratio defines a signed drift parameter, or equivalently a signed Lyapunov exponent, $\gamma(0)$ as

$$\gamma(0) \equiv -\lim_{N \rightarrow \infty} \frac{1}{N} \ln \left| \frac{a_N}{a_1} \right|. \quad (\text{A7})$$

Equivalently, it can also be written as

$$\gamma(0) \equiv \lim_{N \rightarrow \infty} \frac{1}{N} \ln \left| \frac{b_N}{b_1} \right|. \quad (\text{A8})$$

The two expressions are equivalent in the thermodynamic limit, since they describe the same zero-energy bulk drift from opposite recursion directions. The maximal Lyapunov exponent at $E = 0$ is $\lambda(0) = |\gamma(0)|$ [32, 49]. The associated characteristic length is $\xi(0) = 1/\lambda(0)$. When there is a normalizable zero-energy edge mode, $\xi(0)$ coincides with their penetration depth. Substituting the product form into the definition, the logarithm converts

the product into a sum:

$$\begin{aligned}\gamma(0) &= \lim_{N \rightarrow \infty} \frac{1}{N} \sum_{i=1}^{N-1} \ln \left| \frac{t_{2,i}}{t_{1,i+1}} \right| \\ &= \lim_{N \rightarrow \infty} \frac{1}{N} \sum_{i=1}^N \ln \left| \frac{t_{2,i}}{t_{1,i}} \right|.\end{aligned}\quad (\text{A9})$$

We consider the specific case where the inter-cell hopping is uniform ($t_{2,i} = t_2 = 1$) and the intra-cell hopping possesses box-distributed disorder: $t_{1,i} = t_1 + \delta W_i$, where δW_i is a random variable uniformly distributed in the interval $[-W, W]$ with probability density function $P(x) = \frac{1}{2W}$.

According to the Birkhoff ergodic theorem, in the thermodynamic limit ($N \rightarrow \infty$), the spatial average over the chain is equivalent to the ensemble average over the disorder distribution. Thus, Eq. (A9) becomes:

$$\gamma(0) = -\langle \ln |t_1 + \delta W| \rangle = -\int_{-W}^W P(x) \ln |t_1 + x| dx. \quad (\text{A10})$$

The integral can be evaluated analytically, yielding

$$\gamma(0) = \frac{-(t_1 + W) \ln |t_1 + W| + (t_1 - W) \ln |t_1 - W|}{2W} + 1. \quad (\text{A11})$$

This analytical result provides the $\gamma(0)$ as a function of the disorder strength W and the hopping parameter t_1 [49].

For the topological insulator phase ($\langle \ln |t_{2,i}| \rangle > \langle \ln |t_{1,i}| \rangle$), we have $\gamma(0) > 0$. This positive exponent implies that the $E = 0$ eigenstate decays as $|\psi| \sim e^{-\gamma(0) \cdot x}$. Thus, the zero energy states exponentially localize at the two edges; these are the topologically protected edge states, with the localization length $\xi = 1/|\gamma(0)|$. For the trivial insulator phase ($\langle \ln |t_{2,i}| \rangle < \langle \ln |t_{1,i}| \rangle$), we have $\gamma(0) < 0$. This means that any solution to the $E = 0$ eigenstates behaves as $|\psi| \sim e^{-\gamma(0) \cdot x} = e^{|\gamma| \cdot x}$, which grows exponentially in space. Such an exponentially diverging wave function is non-normalizable and therefore does not correspond to a physically acceptable eigenstate. Consequently, no zero energy states exist in the trivial insulator phase. For $\gamma(0) = 0$, the localization length for zero energy is divergent, indicating that the (formerly) zero-energy edge state delocalizes and merges with the bulk states, which is the topological phase transition point. So the transition occurs for $\gamma(0) = 0$. This analytical result yields the critical phase boundary, shown as the solid red line in Fig. 1(a) of the main text, which is fully consistent with the topological phase transition calculated from the real space winding number. For the disorder strength $W = 1.43$ we considered in the main text, $t_1 = 1.40$.

For the parameters considered in Fig. 1(c1,c2) in the main text: $t_1 = 0.29$, $W = 1.43$, the zero-energy edge states in open boundary condition behave as $\langle \ln |\psi|^2 \rangle \sim -2r/\xi$, with the localization length $\xi = 1/\gamma(0) = 1.61$, which is the same as the numerical results in the main text.

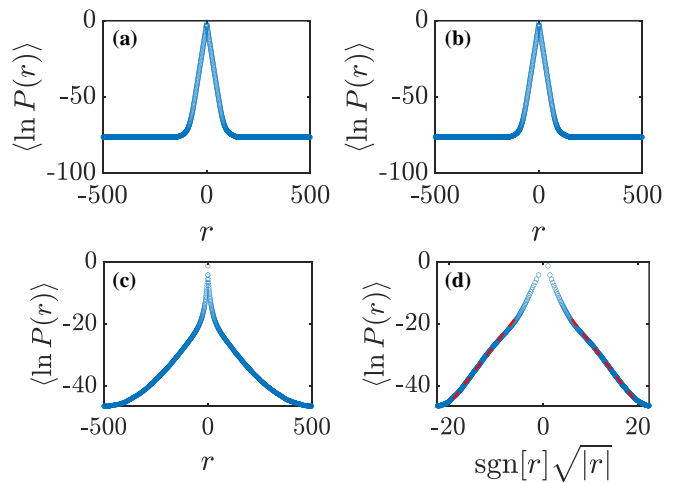


FIG. 6. The logarithm of the eigen states $\langle \ln P(r) \rangle$ for eigen energies windows, (a) for $E \in (0.40, 0.41)$, it is exponential decay. The plateaus are numerical artifacts arising from the machine precision limit of the diagonalization algorithm. (b) for $E \in (-0.41, -0.40)$, it is exponential decay. The plateaus are numerical artifacts arising from the machine precision limit of the diagonalization algorithm. (c) The logarithm of the eigen states $\langle \ln P(r) \rangle$ for eigen energies windows $E \in (-10^{-8}, 10^{-8})$ versus the linear distance r and (d) $\text{sgn}[r]\sqrt{|r|}$. It exhibits a significant departure from the standard exponential decay. Instead, the decay profile is better characterized by subexponential decay. Other parameters are $t_1 = 1.40$, $t_2 = 1$, $N = 1000$, $N_d = 10^4$, $W = 1.43$. Here we consider the periodic boundary condition.

Appendix B: The properties of the Eigenstates

In this part, we discuss the properties of the eigenstates with eigen energies $E \neq 0$ and $E = 0$. For the chiral class, the eigenstate with eigen energy $E \neq 0$ show exponential decay $|\psi| \sim e^{-r/\xi}$ while for eigenstates with eigen energy $E = 0$, their typical profile exhibits subexponential decay [48, 54, 56, 57, 59]. The localization center for every eigenstates are different, we move all the localization centers of the eigenstates to the center unit cell then calculate disorder averaged logarithm of the eigenstates $\langle \ln |\psi(r)|^2 \rangle$. We choose three different eigen energy windows $(0.40, 0.41)$, $(-0.41, -0.40)$, and $(-10^{-8}, 10^{-8})$ for $t_1 = t_1^c = 1.40$. The results of $\langle \ln |\psi|^2 \rangle$ are shown in Fig 6, the eigenstates with $E \neq 0$ ($E \in (0.40, 0.41)$ and $E \in (-0.40, 0.41)$) shown in Fig 6(a,b) exhibit exponential decay with finite localization length. For eigenstates with eigenenergy $E \rightarrow 0$ ($E \in (-10^{-8}, 10^{-8})$), the localization length is divergent [48, 49]. The logarithm of density $\langle \ln P(r) \rangle$ as function of r and $\text{sgn}[r]\sqrt{|r|}$ are shown in 6(c) and (d), respectively. It obviously deviated from the exponential decay; it is subexponential decay. The plateaus in Fig 6(a,b) are numerical artifacts arising from the machine precision limit of the diagonalization algorithm.

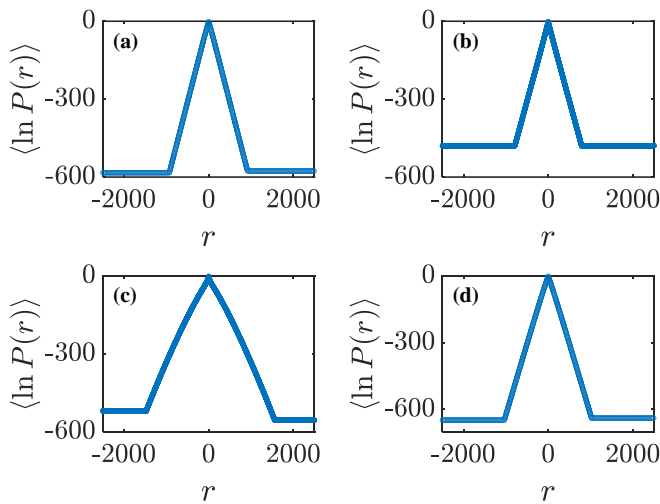


FIG. 7. The disorder averaged the logarithm of the wave density $\langle \ln P(r) \rangle$ for (a) $t_1 = 0.29$ (TI), it is exponentially decay. (b) $t_1 = 1.12$ (TAI), it is also exponentially decay. (c) $t_1 = 1.40$ (CP), the wave packet exhibits non-stationary behavior. (d) $t_1 = 1.90$ (NI), it shows exponential decay. Other parameters are $t_2 = 1$, $N = 5000$, $N_d = 10^4$, $W = 1.43$. The evolution time is $T = 10000$. Here we consider the periodic boundary condition. (Data in the plateaus are absent because the density $\langle \ln P(r) \rangle$ drops below the floating-point precision floor).

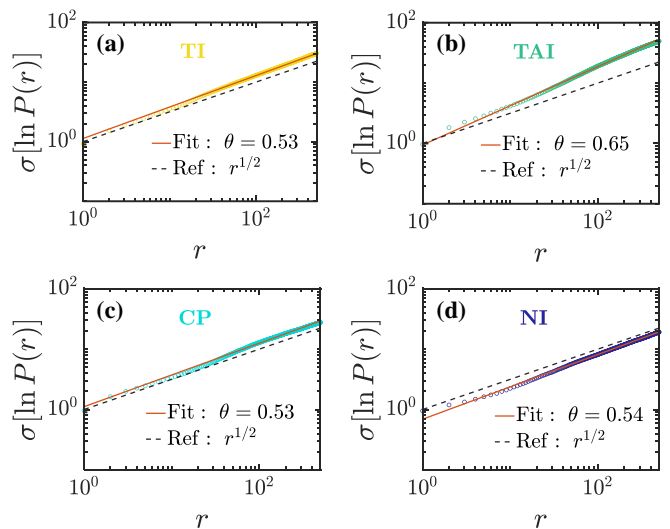


FIG. 8. The fluctuation of the logarithm of the wave density $\ln P(r)$ with distance r . The blue circles represent the numerical data, the solid red line shows a power-law fit, the black dashed line indicates the scaling $y = r/2$ for reference. (a) $t_1 = 0.29$ (TI), the growth exponent is 0.53. (b) $t_1 = 1.12$ (TAI), the growth exponent is 0.65. (c) $t_1 = 1.40$ (CP) at the transition point, the growth exponent is 0.53. (d) $t_1 = 1.90$ (NI), the growth exponent is 0.54. Other parameters are, $t_1 = 1$, $N = 5000$, $N_d = 10000$, $W = 1.43$. The evolution time is $T = 10000$. Here we consider the periodic boundary condition.

Appendix C: More on wavepacket dynamics

To ensure that our results are not finite-size artifacts, we set the number of unit cells to $N = 5000$. The logarithm of the wave density $\ln P(r)$ for different t_1 is shown in Fig. 7 and Fig. 8, the results are same with the result for $N = 1000$.

For the topological and the trivial insulator phase away from the phase transition boundary, the wave packets exponentially decay for large evolution time. The growth exponents for the fluctuation of $\ln P(r)$ are close to $1/2$. For $t_1 = 1.12$ near to the transition, although $\ln P(r)$ still exponentially decay, the growth exponent deviates the Gauss class and increases to 0.65. For the transition point in Fig. 7(c), the wave pack is not exponentially decay. The fluctuation of logarithm is shown in Fig. 8(c), the growth exponent is 0.53. The results for $N = 5000$ are consistent with those for $N = 1000$, indicating that our findings are free from finite-size effects.

-
- [1] J. Li, R.-L. Chu, J. K. Jain, and S.-Q. Shen, Topological anderson insulator, Physical review letters **102**, 136806 (2009).
 [2] E. J. Meier, F. A. An, A. Dauphin, M. Maffei, P. Massignan, T. L. Hughes, and B. Gadway, Observation of the topological anderson insulator in disordered atomic

- wires, Science **362**, 929 (2018).
 [3] S. Stützer, Y. Plotnik, Y. Lumer, P. Titum, N. H. Lindner, M. Segev, M. C. Rechtsman, and A. Szameit, Photonic topological anderson insulators, Nature **560**, 461 (2018).
 [4] G.-G. Liu, Y. Yang, X. Ren, H. Xue, X. Lin, Y.-H. Hu,

- H.-x. Sun, B. Peng, P. Zhou, Y. Chong, *et al.*, Topological anderson insulator in disordered photonic crystals, *Physical Review Letters* **125**, 133603 (2020).
- [5] F. Zangeneh-Nejad and R. Fleury, Disorder-induced signal filtering with topological metamaterials, *Advanced Materials* **32**, 2001034 (2020).
- [6] W. Zhang, D. Zou, Q. Pei, W. He, J. Bao, H. Sun, and X. Zhang, Experimental observation of higher-order topological anderson insulators, *Physical Review Letters* **126**, 146802 (2021).
- [7] H. Liu, B. Xie, H. Wang, W. Liu, Z. Li, H. Cheng, J. Tian, Z. Liu, and S. Chen, Acoustic topological anderson insulators, arXiv preprint arXiv:2111.06520 (2021).
- [8] Q. Lin, T. Li, L. Xiao, K. Wang, W. Yi, and P. Xue, Observation of non-hermitian topological anderson insulator in quantum dynamics, *Nature Communications* **13**, 3229 (2022).
- [9] X.-D. Chen, Z.-X. Gao, X. Cui, H.-C. Mo, W.-J. Chen, R.-Y. Zhang, C. Chan, and J.-W. Dong, Realization of time-reversal invariant photonic topological anderson insulators, *Physical Review Letters* **133**, 133802 (2024).
- [10] M. Ren, Y. Yu, B. Wu, X. Qi, Y. Wang, X. Yao, J. Ren, Z. Guo, H. Jiang, H. Chen, *et al.*, Realization of gapped and ungapped photonic topological anderson insulators, *Physical Review Letters* **132**, 066602 (2024).
- [11] X. Li, H. Xu, J. Wang, L.-Z. Tang, D.-W. Zhang, C. Yang, T. Su, C. Wang, Z. Mi, W. Sun, *et al.*, Mapping the topology-localization phase diagram with quasiperiodic disorder using a programmable superconducting simulator, *Physical Review Research* **6**, L042038 (2024).
- [12] D. Khudaiberdiev, Z. Kvon, M. Ryzhkov, D. Kozlov, N. Mikhailov, and A. Pimenov, Two-dimensional topological anderson insulator in a hgte-based semimetal, *Physical Review Research* **7**, L022033 (2025).
- [13] Z. Li, Z. Chen, D. Kong, Y. Li, K. Cui, X. Feng, and Y. Huang, Demonstration of time-reversal symmetric two-dimensional photonic topological anderson insulator, arXiv preprint arXiv:2501.11251 (2025).
- [14] M. Mannai, Y. Shu, S. Haddad, M. Ren, H. Chen, Y. Sun, and H. Sati, Realization of staircase topological anderson phase transitions, arXiv preprint arXiv:2601.14769 (2026).
- [15] C. Groth, M. Wimmer, A. Akhmerov, J. Tworzydło, and C. Beenakker, Theory of the topological anderson insulator, *Physical review letters* **103**, 196805 (2009).
- [16] H. Jiang, L. Wang, Q.-f. Sun, and X. Xie, Numerical study of the topological anderson insulator in hgte/cdte quantum wells, *Physical Review B—Condensed Matter and Materials Physics* **80**, 165316 (2009).
- [17] H.-M. Guo, G. Rosenberg, G. Refael, and M. Franz, Topological anderson insulator in three dimensions, *Physical review letters* **105**, 216601 (2010).
- [18] A. Altland, D. Bagrets, L. Fritz, A. Kamenev, and H. Schmiedt, Quantum criticality of quasi-one-dimensional topological anderson insulators, *Physical Review Letters* **112**, 206602 (2014).
- [19] L.-Z. Tang, L.-F. Zhang, G.-Q. Zhang, and D.-W. Zhang, Topological anderson insulators in two-dimensional non-hermitian disordered systems, *Physical Review A* **101**, 063612 (2020).
- [20] C. W. Beenakker, Random-matrix theory of quantum transport, *Reviews of modern physics* **69**, 731 (1997).
- [21] P. A. Mello and N. Kumar, *Quantum Transport in Mesoscopic Systems: Complexity and Statistical Fluctuations. A Maximum Entropy Viewpoint* (Oxford University Press, 2004).
- [22] F. Evers and A. D. Mirlin, Anderson transitions, *Reviews of Modern Physics* **80**, 1355 (2008).
- [23] M. L. Mehta, *Random matrices*, Vol. 142 (Elsevier, 2004).
- [24] O. Dorokhov, Transmission coefficient and the localization length of an electron in n bound disordered chains, *Soviet Journal of Experimental and Theoretical Physics Letters* **36**, 318 (1982).
- [25] P. Mello, P. Pereyra, and N. Kumar, Macroscopic approach to multichannel disordered conductors, *Annals of Physics* **181**, 290 (1988).
- [26] K. Muttalib and J. Klauder, Generalized fokker-planck equation for multichannel disordered quantum conductors, *Physical review letters* **82**, 4272 (1999).
- [27] K. Muttalib and V. A. Gopar, Generalization of the dmpk equation beyond quasi one dimension, *Physical Review B* **66**, 115318 (2002).
- [28] A. Douglas, P. Markoš, and K. Muttalib, The generalized dmpk equation revisited: towards a systematic derivation, *Journal of Physics A: Mathematical and Theoretical* **47**, 125103 (2014).
- [29] I. Suslov, General form of dmpk equation, *Journal of Experimental and Theoretical Physics* **127**, 131 (2018).
- [30] A. D. Mirlin, Statistics of energy levels and eigenfunctions in disordered systems, *Physics Reports* **326**, 259 (2000).
- [31] P. W. Anderson, D. Thouless, E. Abrahams, and D. Fisher, New method for a scaling theory of localization, *Physical Review B* **22**, 3519 (1980).
- [32] B. Kramer and A. MacKinnon, Localization: theory and experiment, *Reports on Progress in Physics* **56**, 1469 (1993).
- [33] H. Furstenberg, Noncommuting random products, *Transactions of the American Mathematical Society* **108**, 377 (1963).
- [34] M. Kardar, G. Parisi, and Y.-C. Zhang, Dynamic scaling of growing interfaces, *Physical Review Letters* **56**, 889 (1986).
- [35] A. Somoza, M. Ortuno, and J. Prior, Universal distribution functions in two-dimensional localized systems, *Physical Review Letters* **99**, 116602 (2007).
- [36] G. Lemarié, Glassy properties of anderson localization: Pinning, avalanches, and chaos, *Physical review letters* **122**, 030401 (2019).
- [37] S. Mu, J. Gong, and G. Lemarié, Kardar-parisi-zhang physics in the density fluctuations of localized two-dimensional wave packets, *Phys. Rev. Lett.* **132**, 046301 (2024).
- [38] N. Swain, S. Adam, and G. Lemarié, Two-dimensional anderson localization and kpz subuniversality classes: Sensitivity to boundary conditions and insensitivity to symmetry classes, *Phys. Rev. Res.* **8**, 013038 (2026).
- [39] S. Mu, G. Lemarié, and J. Gong, Universal fluctuations of two localized interacting particles in one dimension, *Phys. Rev. B* **112**, 014201 (2025).
- [40] N. Izem, B. Georgeot, J. Gong, G. Lemarié, and S. Mu, Kardar-parisi-zhang and glassy properties in 2d anderson localization: eigenstates and wave packets, arXiv:2512.12085 (2025).
- [41] W.-P. Su, J. R. Schrieffer, and A. J. Heeger, Solitons in polyacetylene, *Physical review letters* **42**, 1698 (1979).
- [42] P. W. Anderson, Absence of diffusion in certain random lattices, *Physical review* **109**, 1492 (1958).

- [43] A. Lagendijk, B. v. Tiggelen, and D. S. Wiersma, Fifty years of anderson localization, *Physics today* **62**, 24 (2009).
- [44] N. F. Mott and W. Twose, The theory of impurity conduction, *Advances in physics* **10**, 107 (1961).
- [45] E. Abrahams, P. W. Anderson, D. C. Licciardello, and T. V. Ramakrishnan, Scaling theory of localization: Absence of quantum diffusion in two dimensions, *Physical Review Letters* **42**, 673 (1979).
- [46] R. Borland, The nature of the electronic states in disordered one-dimensional systems, *Proceedings of the Royal Society of London. Series A. Mathematical and Physical Sciences* **274**, 529 (1963).
- [47] L. Fleishman and D. Licciardello, Fluctuations and localization in one dimension, *Journal of Physics C: Solid State Physics* **10**, L125 (1977).
- [48] C. Soukoulis and E. Economou, Off-diagonal disorder in one-dimensional systems, *Physical Review B* **24**, 5698 (1981).
- [49] I. Mondragon-Shem, T. L. Hughes, J. Song, and E. Prodan, Topological criticality in the chiral-symmetric aiii class at strong disorder, *Physical review letters* **113**, 046802 (2014).
- [50] G. De Tomasi, S. Roy, and S. Bera, Generalized dyson model: Nature of the zero mode and its implication in dynamics, *Physical Review B* **94**, 144202 (2016).
- [51] F. J. Dyson, The dynamics of a disordered linear chain, *Physical Review* **92**, 1331 (1953).
- [52] M. Weissmann and N. Cohan, Density of states of a one-dimensional system with off-diagonal disorder, *Journal of Physics C: Solid State Physics* **8**, L145 (1975).
- [53] R. Bush, On the anomalous behaviour at the band centre of a one-dimensional system with off-diagonal disorder, *Journal of Physics C: Solid State Physics* **8**, L547 (1975).
- [54] G. Theodorou and M. H. Cohen, Extended states in a one-dimensional system with off-diagonal disorder, *Physical Review B* **13**, 4597 (1976).
- [55] T. Eggarter and R. Riedinger, Singular behavior of tight-binding chains with off-diagonal disorder, *Physical Review B* **18**, 569 (1978).
- [56] T. A. Ziman, Localization with off-diagonal disorder: A qualitative theory, *Physical Review B* **26**, 7066 (1982).
- [57] M. Hilke, The disordered su-schrieffer-heeger model, *arXiv preprint arXiv:2512.24738* (2025).
- [58] P. W. Brouwer, C. Mudry, and A. Furusaki, Density of states in coupled chains with off-diagonal disorder, *Physical Review Letters* **84**, 2913 (2000).
- [59] L. Balents and M. P. Fisher, Delocalization transition via supersymmetry in one dimension, *Physical Review B* **56**, 12970 (1997).
- [60] L.-Z. Tang, S.-N. Liu, G.-Q. Zhang, and D.-W. Zhang, Topological anderson insulators with different bulk states in quasiperiodic chains, *Physical Review A* **105**, 063327 (2022).
- [61] J. K. Asbóth, L. Oroszlány, and A. Pályi, *A short course on topological insulators*, Vol. 919 (Springer, 2016).
- [62] J. Billy, V. Josse, Z. Zuo, A. Bernard, B. Hambrecht, P. Lugan, D. Clément, L. Sanchez-Palencia, P. Bouyer, and A. Aspect, Direct observation of anderson localization of matter waves in a controlled disorder, *Nature* **453**, 891 (2008).
- [63] G. Roati, C. D'Errico, L. Fallani, M. Fattori, C. Fort, M. Zaccanti, G. Modugno, M. Modugno, and M. Inguscio, Anderson localization of a non-interacting bose-einstein condensate, *Nature* **453**, 895 (2008).
- [64] J. Prior, A. Somoza, and M. Ortuno, Conductance fluctuations and single-parameter scaling in two-dimensional disordered systems, *Physical Review B—Condensed Matter and Materials Physics* **72**, 024206 (2005).
- [65] J. Prior, A. Somoza, and M. Ortuno, Conductance distribution in two-dimensional localized systems with and without magnetic fields, *The European Physical Journal B* **70**, 513 (2009).
- [66] A. Somoza, P. Le Doussal, and M. Ortuno, Unbinding transition in semi-infinite two-dimensional localized systems, *Physical Review B* **91**, 155413 (2015).
- [67] A. Krishna and R. N. Bhatt, Beyond universal behavior in the one-dimensional chain with random nearest-neighbor hopping, *Physical Review B* **101**, 224203 (2020).